Coordinative Alignment in the Pores of MOFs for the Structural Determination of N-, S-, and P-Containing Organic Compounds Including Complex Chiral Molecules

Xiaokun Pei,[†] Hans-Beat Bürgi,[‡,§] Eugene A. Kapustin,[†] Yuzhong Liu,[†] and Omar M. Yaghi*[⊥,†]

[†]Department of Chemistry, University of California-Berkeley; Materials Sciences Division, Lawrence Berkeley National Laboratory; and Kavli Energy NanoSciences Institute, Berkeley, California 94720, United States

[‡]Department of Chemistry and Biochemistry, Universität Bern, Freiestrasse 3, CH-3012 Bern, Switzerland

[§]Department of Chemistry, University of Zurich, Winterthurestrasse 190, CH-8057 Zurich, Switzerland

[⊥]UC Berkeley-KACST Joint Center of Excellence for Nanomaterials for Clean Energy Applications, King Abdulaziz City for Science and Technology, Riyadh 11442, Saudi Arabia

S *Supporting Information*

ABSTRACT: Coordinative alignment of target small molecules onto a chiral metal–organic framework (MOF-520)-provides a powerful method to determine the structures of small molecules through single-crystal X-ray diffraction (SXRD). In this work, the structures of 17 molecules with eight new coordinating functionalities and varying size have been determined by this method, four of which are complex molecules being crystallized for the first time. The chirality of the MOF backbone not only enables enantioselective crystallization of chiral small molecules from a racemic mixture but also imposes diastereoselective incorporation upon achiral molecules. Crystallographic studies assisted by density functional theory (DFT) calculations indicate that the stereoselectivity of MOF-520 not exclusively comes from the steric confinement of the chiral pore environment but also from asymmetric chemical bonding of the target molecules with the framework that is able to provide sufficient energy difference between possible coordination configurations.
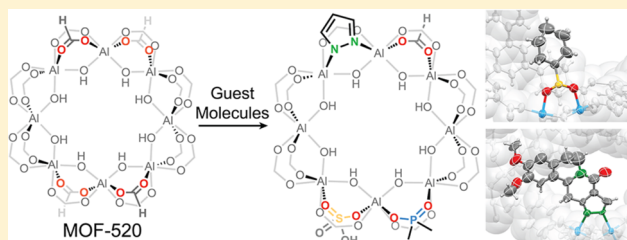
INTRODUCTION

Single-crystal X-ray diffraction (SXRD) analysis is a powerful technique to determine the spatial arrangement of molecules with atomic precision. While single crystals for most common molecules can be obtained, it remains a problem when the amount of material is limited, the crystal quality is poor, and the target molecule is complex and of irregular geometry. In 2016, our group reported the coordinative alignment (CAL) method: It involves the coordinative attachment of the molecule of interest to the backbone of a chiral metal–organic framework (MOF), MOF-520.[1,2] In this way the crystallinity of the MOF allows determination of the single-crystal X-ray structure and absolute configuration of the bound molecule. This method provides a number of advantages: (1) The coordinative attachment of target molecules to the framework backbone decreases their motional degrees of freedom and aligns them into an ordered pattern within the MOF, thus facilitating their structural determination and (2) each of the two enantiomorphs of chiral MOF-520 (Δ and Λ) can selectively crystallize one of the enantiomers from a racemic mixture of target molecules. In contrast to previously reported methods,[3–5] the CAL method is enabled by strong bonding that anchors the functional groups of the target molecule onto the framework, in addition to weak interactions between the

molecule and the framework that help in steadying the former. To be suitable for structure solution using the CAL method, target molecules need to bear functional groups that can coordinate to metal sites of the framework's secondary building units (SBUs, Al³⁺ in the case of MOF-520). As such, expanding the scope of suitable coordinating functionalities is paramount to gaining access to structural data of a library of chiral and complex organic molecules that are difficult to crystallize on their own.

In this work, molecules containing three new categories of functionalities; namely, nitrogen-containing azolates, sulfur-containing oxoacids, and phosphorus-containing oxoacids (Scheme 1a) were successfully crystallized in MOF-520. The precise structures of 17 molecules with these functionalities were unambiguously determined, four of which are complex molecules being crystallized for the first time. The high robustness of MOF-520 allows solvent in the pores to be evacuated and ensure better definition of the structures of the target molecule at low occupancy. Compared to solvated structures, these molecules were better aligned and the electron density background due to solvent molecules was

Scheme 1. (a) Newly-Incorporated Functional Groups, (b) Illustration of Their Binding Modes, and (c) Target Molecules

a)

Azolates

pyrazole   triazole   imidazole   tetrazole

N—NH   N—NH   N—NH   N—NH

Sulfur Oxoacids

sulfinic acid   sulfuric acid

Phosphorous Oxoacids

phosphinic acid   phosphonic acid   phosphorous acid

b)

c)

17   18   19   20   21   22   23   24

25   26   27   28   29   30   31

(S)-32   (R)-32   31
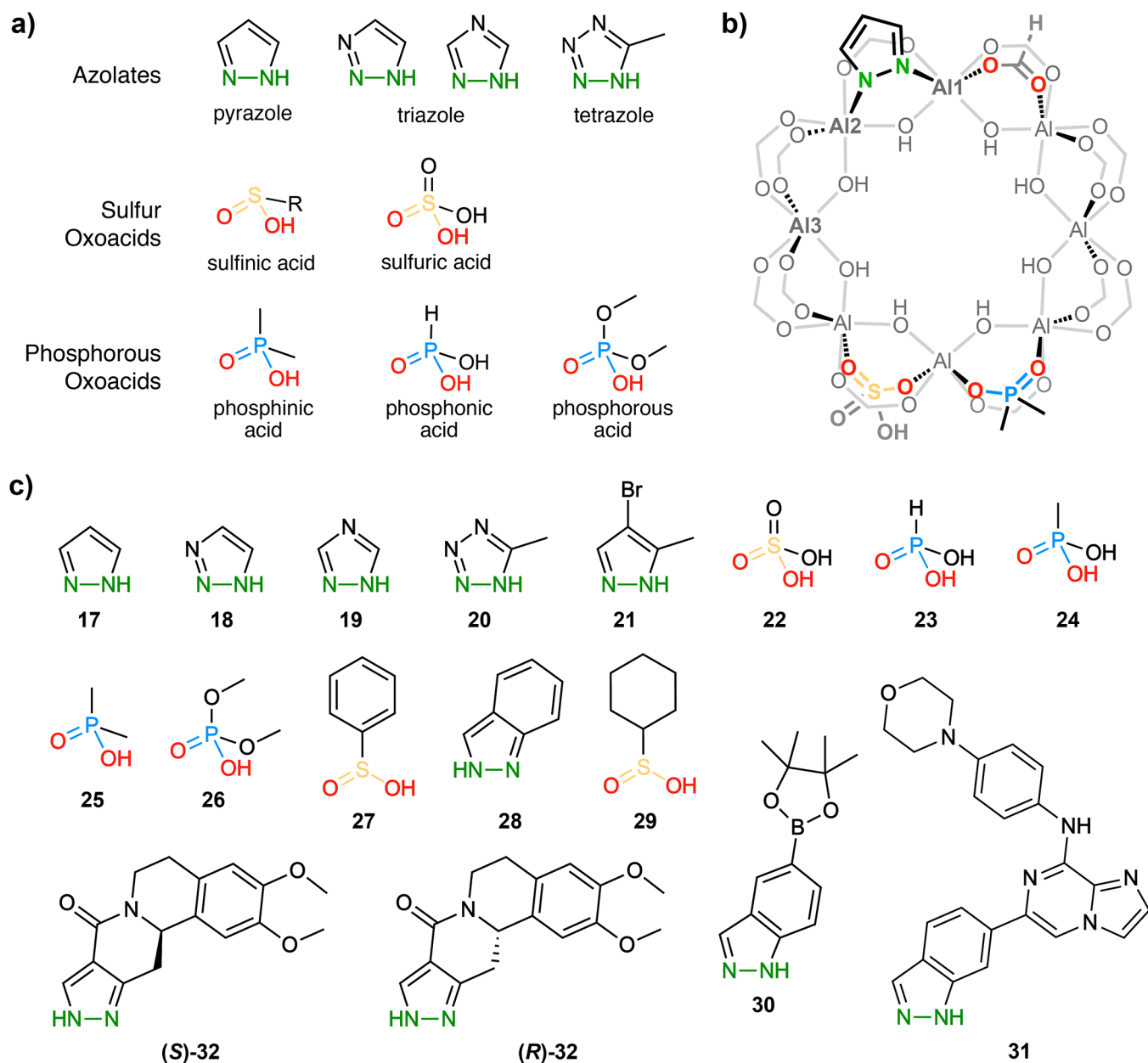
significantly reduced. The stereoselectivity induced by the chirality of MOF-520 was further studied. The chiral host not only enables high selectivity toward one enantiomer of a racemic mixture but also imposes diastereoselective incorporation of achiral molecules to crystallize in specific orientations. Indeed, the stereoselectivity of MOF-520 stems from asymmetric chemical bonding in addition to previously observed steric and intermolecular interactions of the chiral pore environment.[1]

■ EXPERIMENTAL SECTION

General Procedure for Incorporation of Target Molecules. Nitrogen-containing azolates were incorporated into MOF-520 by immersion of pristine MOF-520 in 0.1−1 mol L^{-1} *N,N*-dimethylformamide (DMF) solutions at 85−100 °C for 2 or 3 days. Sulfur oxoacids were incorporated by immersion in 0.3−0.6 mol L^{-1} solutions at 85−100 °C for 1 or 2 days. Phosphorus oxoacids were incorporated by immersion in 0.005−0.015 mol L^{-1} solutions at

−20 to 0 °C for 2 or 3 days. Detailed procedures for all incorporated molecules are provided in the Supporting Information (SI), section S1.

Single-Crystal X-ray Diffraction. Single crystal data were collected at beamlines 11.3.1/12.2.1 at the Advanced Light Source and a Bruker D8 Venture diffractometer. Single crystals were mounted in a 100(2) K nitrogen cold stream. The data up to sin(θ)/λ = 2/3 were collected with combined phi and omega scans to ensure a data multiplicity of at least 8. The raw data were processed with the Bruker APEX3 V8.38 software package.[6] The data were first integrated using SAINT and then corrected for absorption with SADABS.[7] The structures were solved by direct methods (SHELXS) and the refinements done by full-matrix least-squares on F^2 (SHELXL),[8,9] using the Olex^2 software package.[10] Solvent masking was applied to nonactivated structures.[11,12] Parameters indicating data quality fall into the following ranges: resolution, 0.75−0.91 Å; R_{int}, 3.67%−11.82%; R, 2.74%−14.65%; Flack parameter, −0.06(5) to 0.230(11); standard uncertainties of C−C bond lengths, 0.0020−0.0152 Å. Observed structure factor (F_{obs}) electron density maps were
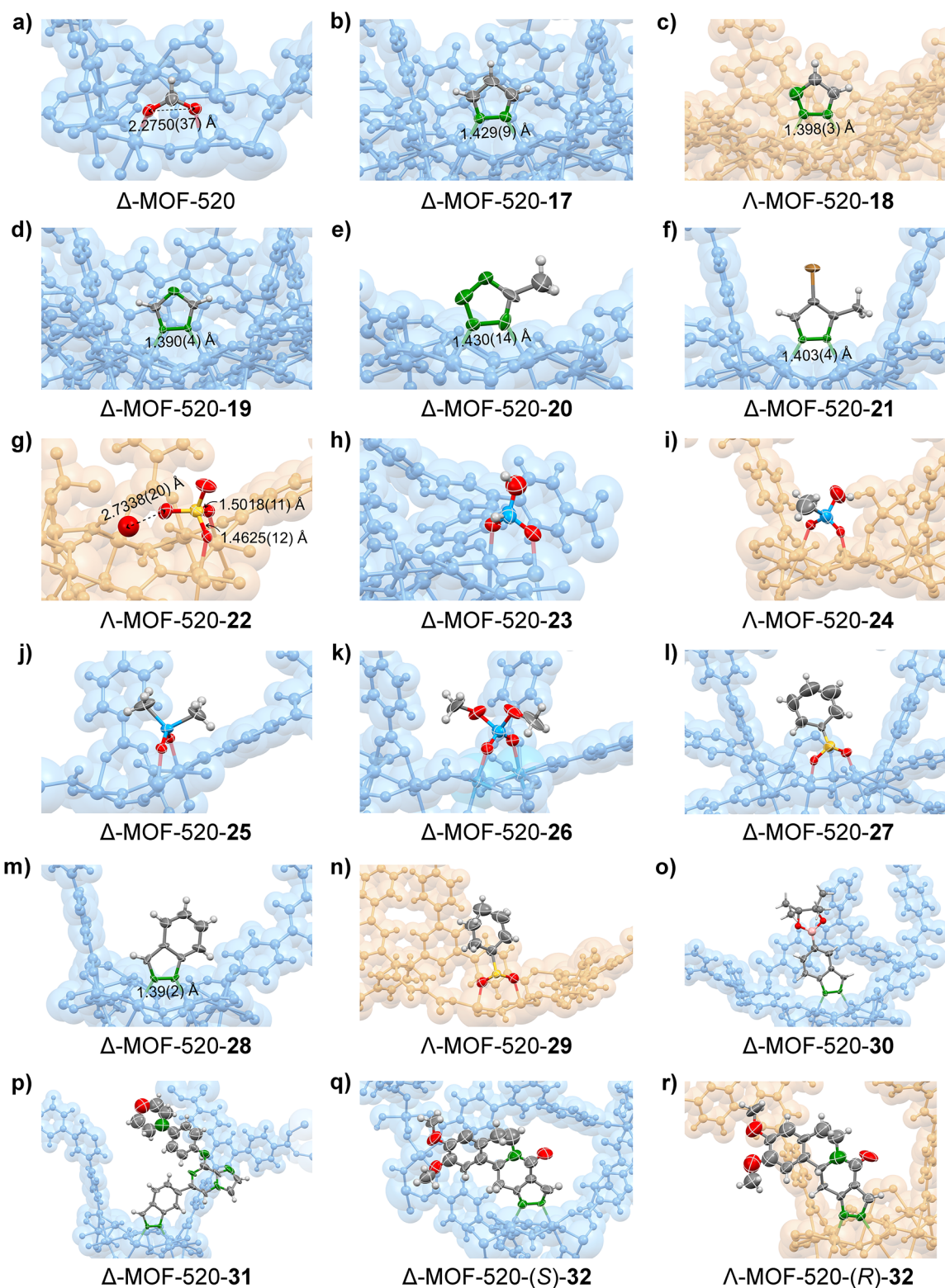
Figure 1. (a) Structure of Δ-MOF-520 showing the formate group to be replaced by target molecules. (b−r) Refined structures of **17** to **32** crystallized in Δ- or Λ-MOF-520. The refined structures of the molecules obtained from SXRD data are illustrated with 50% probability thermal ellipsoids. The distances between coordinating atoms are marked in (a−f) and (m). Bond lengths and possible hydrogen bonding is indicated in (g). In the case of positional disorder, only one conformation of the bound molecules is shown for clarity (c, h, n−r). Color code: blue, Al; orange, P; yellow, S; red, O; green, N; dark gray, C; pink, B; gray, H. The MOF backbone in the figures was drawn as blue (for Δ-MOF-520) or orange (for Λ-MOF-520) space-filling model.

computed in GSAS-II[13] and visualized in VESTA 3.[14] Details for each

structure determination are available in the SI, section S3.

Computational Methods. Calculations on molecular models of the secondary building unit (SBU) were performed using Gaussian 16 (revision A03).[15] The dispersion-corrected PBE0-D3(BJ)[16,17] func-

tional in combination with mixed basis sets [def2-SVP, def2-SVPD, def2-SV(P), and def2-TZVP][18,19] were used in the calculations. All other computations were performed with CrystalExplorer17[20] using a local implementation of B3LYP-D2/6-31G(d,p). Full details are available in the SI, sections S5 and S6.

■ RESULTS AND DISCUSSION

MOF-520 crystallizes in the Sohncke space group $P4_22_12$. Each MOF-520 crystal is enantiopure (labeled as Δ or Λ) but the batch is a racemic mixture of both enantiomorphs of MOF-520. The SBUs of the framework are composed of eight aluminum octahedra in a circular arrangement with 222 point symmetry.[21] Each pair of adjacent aluminum atoms is bridged by one μ_2-OH and two carboxylate groups (Figure S3, Scheme 1b). Out of the 16 μ_2-COO at each SBU, 12 are contributed by the organic linker 1,3,5-benzentribenzoate (BTB), and four are formate ligands that can be exchanged by incoming target molecules with coordinating functionalities. The different carboxylates provide the aluminum atoms with three different chemical environments: Al1 is coordinated to two formates and two BTBs, Al2 is coordinated to one formate and three BTBs, while Al3 is coordinated to four BTBs.

Incorporation of Target Molecules with N-, S-, P-containing Functionalities. In this work, molecules of eight new classes of coordination moieties were introduced into MOF-520, including pyrazole, triazole, tetrazole, sulfuric acid, sulfinic acid, phosphinic acid, phosphonic acid, and phosphoric acid (Scheme 1a). As a result, 17 molecules were incorporated into MOF-520: 1H-pyrazole **17**, 1H-1,2,3-triazole **18**, 1H-1,2,4-triazole **19**, 5-methyl-1H-tetrazole **20**, 4-bromo-3-methyl-1H-pyrazole **21**, sulfuric acid **22**, phosphonic acid **23**, methylphosphonic acid **24**, dimethylphosphinic acid **25**, dimethyl phosphate **26**, phenylsulfinic acid **27**, 1H-indazole **28**, cyclohexanesulfinic acid **29**, 1H-indazole-5-boronic acid pinacol ester **30**, Entospletinib[22] **31**, and 2,3-dimethoxy-5,11,12,12a-tetrahydropyrazolo[3′,4′:4,5]pyrido[2,1-a]-isoquinolin-8(6H)-one [(S)-**32** and (R)-**32**]. Among them, compounds **30**, **31**,(S)-**32** and (R)-**32** were crystallized for the first time (Scheme 1c).

The incorporation temperatures, concentrations, and reaction times were similar within each respective group of N-, S-, and P-containing molecules. Molecules with nitrogen-containing azolates were introduced into MOF-520 as 0.15−1 mol L^{-1} solutions at 85 °C, while sulfur oxoacids were incorporated at lower concentrations (0.033−0.06 mol L^{-1}) and phosphorus oxoacids were introduced at lower temperatures of 0 °C or −20 °C due to different ligand binding strength. Lower temperatures and concentrations decrease the diffusion rate of molecules within the pores of the MOF. Therefore, the loading of phosphorus oxoacids is approximately 25−70%, while the azolate-bonded molecules generally show higher loadings (50−100%) with the exception of sterically bulky molecules (Table S1).

Single-Crystal X-ray Diffraction Studies of Molecule-Incorporated MOF-520: General Observations. The high structural and chemical stability of MOF-520 facilitates ligand substitution while preserving crystallinity of the backbone. Both the space group and enantiomorph of MOF-520 remain unchanged since the incoming ligands bind to the MOF in the same μ_2-bridging fashion as the replaced formates (Scheme 1b). The changes of the unit cell parameters of MOF-520 upon binding of the molecules serve as a first indicator of incorporation. In pristine MOF-520, the unit cell parameters

are approximately 18.58 Å × 18.58 Å × 37.30 Å. On substituting the formates by azolates, the c axis of azolate-incorporated MOF-520 is shortened to ∼35.7 Å, while the a and b axes elongate to ∼19.5 Å (Table S1). This can be traced to the change of distance between the coordinating atoms (i.e., ∼2.3 Å between the oxygen atoms of formates, but ∼1.4 Å between nitrogen atoms of azolates, Figure 1a−f, m), which leads to a distortion of the SBU and consequently of the entire unit cell. For similar reasons, the a and b axes are slightly longer in sulfur and phosphorus oxoacids, whereas the c axis is slightly shorter: the unit cell parameters of Λ-MOF-520-**29** are a = 18.7011(9) Å and c = 37.206(2) Å and of Δ-MOF-520-**25**, a = 18.9892(8) Å and c = 36.9796(15) Å (Table S1).

The connectivity and conformations of incorporated molecules were determined with atomic precision (Figure 1). Sulfinic acids are known to have a trigonal pyramidal sulfur configuration. Correspondingly, in molecules **27** and **29**, the cyclohexyl and phenyl groups were observed to bend out of the O−S−O plane (Figure 1l,n). Sulfuric acid (**22**) retains its tetrahedral geometry and coordinates to MOF-520 through one double-bonded oxygen and one deprotonated hydroxyl oxygen, as corroborated by the observed bond lengths [1.4625(12) Å and 1.5018(11) Å; Figure 1g].[23−25] The presence of an oxygen atom from a solvent molecule inside of the MOF's pore was also observed, and its distance to the closest oxygen atom of **22** is ∼2.73 Å, indicating hydrogen bonding between **22** and solvent which energetically stabilizes the position of the target molecule (SI, section S3.2.8). Phosphorus oxoacids **24**, **25**, and **26** also display the common tetrahedral geometry of the phosphorus atom. In the case of Δ-MOF-520-**23**, the atomic displacement parameters (ADPs) of the atoms in **23** are relatively large and a nearly planar geometry of the central phosphorus atom is observed, suggesting that **23** aligns in mixed orientations or possibly as mixed tautomers (SI, section 3.2.9).[26,27] In contrast, **24** definitely shows a tetrahedral phosphorus atom with a significant distinction between the P−OH (noncoordinating hydroxyl) and P−C bond lengths [1.527(4) and 1.987(8) Å, respectively; SI, section 3.2.11].

Incorporated MOF-520 Crystals with and without Solvent. Incorporated MOF-520 crystals with low target molecule occupancy were evacuated prior to SXRD measurements because additional solvent molecules in the pore will (1) tend to form disordered structures due to flash cooling and thus contributing to positional disorder of the target molecules[28] and (2) increase background electron densities, implying the risk of ambiguous atom assignment of target molecules. The solvent removal becomes possible because of the high architectural stability of MOF-520, which enables full retention of its crystallinity throughout incorporation, activation procedure and the SXRD measurement. Here we compare F_{obs} (observed structure factor) electron density maps before and after activation of MOF-520-**30** and MOF-520-**31**, respectively, and the results illustrate that solvent removal is advantageous for the determination of unknown crystal structures of molecules **30** and **31** (Figure 2).

Δ-MOF-520-**30** was first measured in the presence of DMF at 100 K. Continuous electron densities representing continuous disordered positions between two modeled positions are observed for this structure (Figure 2a), posing challenges for the refinement of atomic coordinates and ADPs of the planar indazole fragment. Moreover, the pinacol ester could not be modeled. Upon activation, the positional disorder
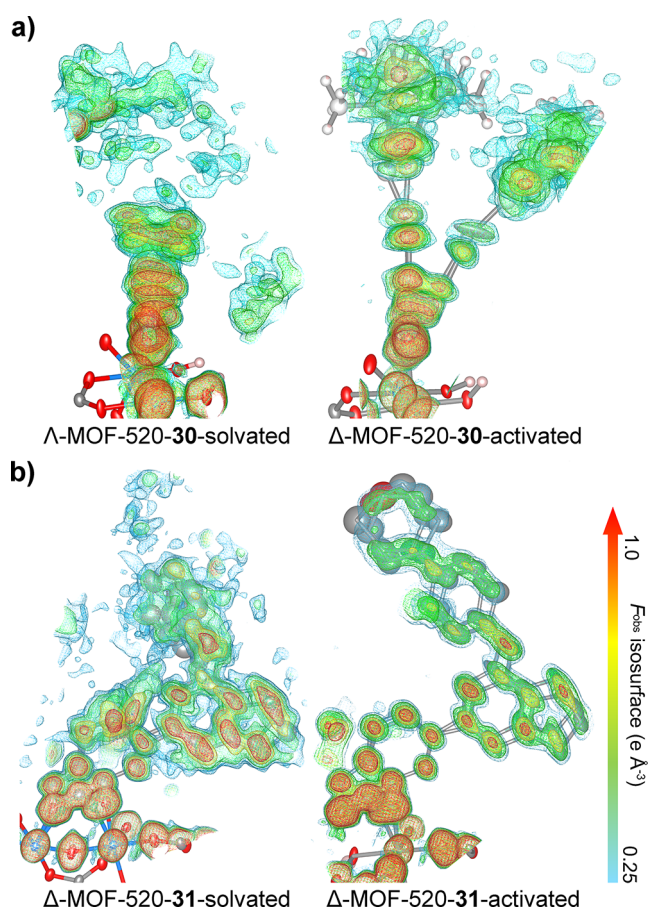
Figure 2. F_{obs} electron density isosurface plots for MOF-520-**30** and MOF-520-**31** before and after solvent evacuation. The plot is overlaid with the structure model. Color code of structure models: Al, blue; O, red; N, green; C, gray; B, purple; and H, pink.

Figure 3. (a) Illustration of the chiral volume determined for the structures (*S*)-**32** and (*R*)-**32**. (b) The measured dihedral angle between the planes A and D (filled in blue) in (*S*)-**32** and (*R*)-**32**. Color code for atoms: O, red; N, green; C, gray; and H, pink. Subscript A, B in the angle notations refers to A and B position of **32** in the SXRD structures (SI, sections 3.2.21 and 3.2.22).

of the molecule is reduced to only two distinct positions, allowing for unambiguous structure modeling and full structural resolution of **30**.

The solvent molecules which are present in porous structures inevitably form a background of electron densities with average levels of 0.2–0.4 e $Å^{-3}$,[12,29] which overlaps with the electron density of low occupancy incorporated molecules. For example, Δ-MOF-520-**31**-solvated and Δ-MOF-520-**31**-activated were solved with molecule occupancies of 36% and 26%, respectively. Comparison of the F_{obs} maps of the two structures reveal that the structure of **31** is obscured in the solvated MOF due to smeared out electron densities contributed by the solvent molecules, but becomes better defined upon activation of the framework (electron density distribution matches the incorporated molecule; Figure 2b).

Enantiomeric Discrimination of a Racemic Mixture by Incorporation into MOF-520. Enantiomeric separation was demonstrated for a racemic mixture of (*S*)-**32** and (*R*)-**32**. A racemic batch of MOF-520 crystals was immersed into a 0.2 mol L^{-1} DMF solution and kept at 85 °C for 3 days, then washed with fresh solvents and activated. Single crystal structures of molecule-incorporated Δ- and Λ-MOF-520 crystals were subsequently determined. In both MOF structures, two disordered, homochiral molecules were modeled (~25% occupancy for each); from which it is concluded that (*S*)-**32** coordinates to Δ-MOF-520 only, while (*R*)-**32** coordinates exclusively to Λ-MOF-520 (Figure 1q,r).

The reliability of the assigned absolute configuration of the molecule structures was confirmed by analyzing the chiral volume of the chiral carbon (C32, Figure 3a). As a point of reference, the chiral volume of the chiral center in amino acids is ±2.492 $Å^3$.[30] The chiral volumes of C32 of the two positions in each framework were measured to be −2.20 (0.19) and −1.94 (0.20) $Å^3$ in Δ-MOF-520-(*S*)-**32**, +2.07 (0.18) and +1.71 (0.24) $Å^3$ in Λ-MOF-520-(*R*)-**32**, three of which are within 3σ of the ideal value. Additionally, enantiopurity of the incorporated molecules in each framework was corroborated by analyzing their conformations. The different chiralities of C32 induce mirrored conformations of the two six-membered rings (B and C, Figure 3b), resulting in dihedral angles between the benzene ring D and pyrazole ring A of opposite sign (Figure 3b). In both structures no residual electron density attributable to the other enantiomer was observed, further substantiating that MOF-520 can be highly selective toward one enantiomer of racemic mixtures.

Diastereoselective Incorporation on Prochiral Target Molecules. The chirality of the host framework not only displays enantioselective incorporation toward chiral molecules, but also imposes diastereoselective coordination on prochiral molecules. Here, prochiral molecules are aligned in a specific asymmetric orientation, leading to just one of the two possible diastereomers for each enantiomorph of host MOF-520 (SI, section S4). The binding of the spatially bulkier azoles **20**, **21**, **28**, **30**, **31**, (*S*)-**32**, (*R*)-**32**, can be attributed to steric selectivity, however, the selectivity was also observed in smaller molecules that are minimally influenced by steric hindrance.

Methylphosphonic acid (**24**) and 1*H*-1,2,3-triazole (**18**) can potentially adopt two different configurations upon coordination to one enantiomorph of MOF-520 and form two diastereomers of the molecule-incorporated framework. However, only one preferred orientation is consistently observed in a given enantiomorph. The noncoordinating hydroxyl group in **24** always points to the center of the SBU, while the methyl group points in the opposite direction (Figure 4a). Similarly, one specific orientation is observed to
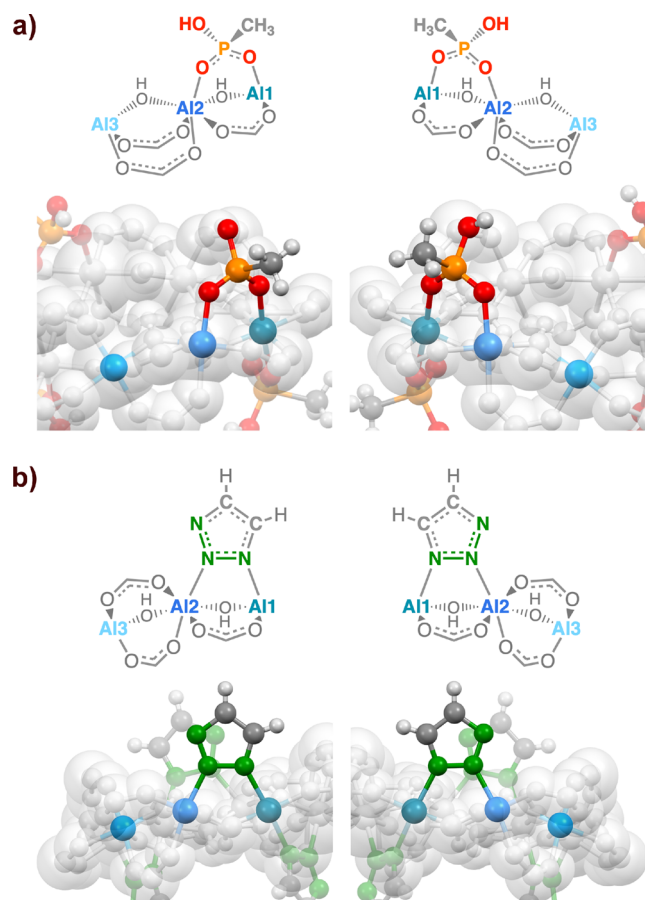
Figure 4. (a) Local structure of the coordination site of methylphosphonic acid in Δ-MOF-520-**24** and Λ-MOF-520-**24**. (b) Local structure of the coordination site of 1*H*-1,2,3-triazole in Δ-MOF-520-**18** and Λ-MOF-520-**18**. The blue colors at different levels are used to illustrate the Al atoms of different environment: Al1, turquoise; Al2, aqua blue; and Al3, violet blue. The SBUs except for bound molecules are represented by gray space-filling models. Color code: P, orange; O, red; N, green; C, gray; H, light gray.

be much more preferred than the other in both Δ-MOF-520-**18** and Λ-MOF-520-**18** (Figure 4b). The results are supported by refining the occupancies of the two overlapping positions through free variables. The occupancies of the two possible orientations converged to 0.680(4) and 0.038(4) for Δ-MOF-520-**18** and to 0.632(4) and 0.025(4) for Λ-MOF-520-**18**. In order to understand the driving force that leads to the preferred orientation, possible van der Waals interactions between **18** and the host framework were examined by Hirshfeld surface analysis;[31] however, no significant intermolecular repulsion or attraction was observed between molecule **18** and the MOF (SI, section S5).[32] The lack of the above-mentioned factors leads us to think about the

difference in the Al−N coordination bonds. When the two different N atoms of **18** bind to MOF-520, they bridge two aluminum ions in different chemical environments (Al1 and Al2). The two different sets of Al−N bonds resulting from the two different azole orientations may have different bond strengths. Calculations were performed on the molecular models of the incorporation site, with favored and unfavored orientation of coordinated **18** (SI, section S6). Total energies of the models were obtained from density functional theory (DFT) calculations with polarized continuum model (PCM) accounting for solvent effects. The energy difference in favor of the observed orientation is ca. 8 kJ mol⁻¹ for DMSO and acetone and is primarily attributed to the asymmetric coordinative bonding after solvent stabilization. Accordingly, the stereoselectivity of MOF-520 is not exclusively due to steric effects and weak van der Waals interactions, but also because of asymmetric coordination bonding which causes a sufficient energy difference between the two alternative orientations of the bound molecules.

CONCLUSION AND OUTLOOK

Unambiguous structural determination of 17 molecules with eight new functionalities are provided using the coordinative alignment method. Structures of four of these molecules have never been determined by single-crystal X-ray diffraction. The quality of the single-crystal structural solutions is drastically improved by removing residual solvent from the MOF's pores without deteriorating the crystallinity of its backbone. Stereoselectivity studies with chiral MOF system show enantioselective inclusion from a racemic mixture of target molecules, and diastereoselective binding of prochiral molecules. Our study provides insight into the origin of these selectivities, which are not only due to steric factors or intermolecular interactions but are also strongly influenced by asymmetric coordinative bonding. We believe that, with a broader functionality scope, the CAL method will become a powerful platform for the structure determination of unknown biomolecules, complex chiral natural products, and drug molecules.

ASSOCIATED CONTENT

Ⓢ Supporting Information

The Supporting Information is available free of charge on the ACS Publications website at DOI: 10.1021/jacs.9b10501.

Crystal structure of Λ-MOF-520-30-solvated (CIF)
Crystal structure of Δ-MOF-520-30-activated (CIF)
Crystal structure of Δ-MOF-520-31-solvated (CIF)
Crystal structure of Δ-MOF-520-31-activated (CIF)
Crystal structure of Δ-MOF-520-S-32 (CIF)
Crystal structure of Λ-MOF-520-R-32 (CIF)

■ AUTHOR INFORMATION

Corresponding Author
*yaghi@berkeley.edu

ORCID 🟢
Xiaokun Pei: 0000-0002-6074-1463
Eugene A. Kapustin: 0000-0003-4095-9729
Yuzhong Liu: 0000-0001-5614-1951
Omar M. Yaghi: 0000-0002-5611-3325

Notes
The authors declare no competing financial interest.

■ ACKNOWLEDGMENTS

■ REFERENCES

(1) Lee, S.; Kapustin, E. A.; Yaghi, O. M. Coordinative Alignment of Molecules in Chiral Metal-Organic Frameworks. *Science* **2016**, *353*, 808−811.

(2) Yaghi, O. M.; Kalmutzki, M. J.; Diercks, C. S. *Introduction to Reticular Chemistry: Metal-Organic Frameworks and Covalent Organic Frameworks*; Wiley-VCH: Weinheim, 2019.

(3) *Crystallography of Supramolecular Compounds*; Tsoucaris, G., Atwood, J. L., Lipkowski, J., Eds.; Kluwer Academic Publishers: Dordrecht, The Netherlands, 1996.

(4) Inokuma, Y.; Yoshioka, S.; Ariyoshi, J.; Arai, T.; Hitora, Y.; Takada, K.; Matsunaga, S.; Rissanen, K.; Fujita, M. X-ray analysis on the Nanogram to Microgram Scale Using Porous Complexes. *Nature* **2013**, *495*, 461−466.

(5) Yan, K.; Dubey, R.; Arai, T.; Inokuma, Y.; Fujita, M. Chiral Crystalline Sponges for the Absolute Structure Determination of Chiral Guests. *J. Am. Chem. Soc.* **2017**, *139*, 11341−11344.

(6) *APEX3*, version 8.38; Bruker-AXS: Madison, WI, 2018.

(7) *SADABS*, version 2014/4; Bruker-AXS: Madison, WI, 2014.

(8) Sheldrick, G. M. A Short History of *SHELX*. *Acta Crystallogr., Sect. A: Found. Crystallogr.* **2008**, *64*, 112−122.

(9) Sheldrick, G. M. Crystal Structure Refinement with *SHELXL*. *Acta Crystallogr., Sect. C: Struct. Chem.* **2015**, *71*, 3−8.

(10) Dolomanov, O. V.; Bourhis, L. J.; Gildea, R. J.; Howard, J. A. K.; Puschmann, H. OLEX2: A Complete Structure Solution, Refinement and Analysis Program. *J. Appl. Crystallogr.* **2009**, *42*, 339−341.

(11) Jiang, J.-S.; Brünger, A. Protein Hydration Observed by X-ray Diffraction Solvation Properties of Penicillopepsin and Neuraminidase Crystal Structures. *J. Mol. Biol.* **1994**, *243*, 100−115.

(12) Rees, B.; Jenner, L.; Yusupov, M. Bulk-solvent Correction in Large Macromolecular Structures. *Acta Crystallogr., Sect. D: Biol. Crystallogr.* **2005**, *61*, 1299−1301.

(13) Toby, B. H.; Von Dreele, R. B. GSAS-II: the Genesis of a Modern Open-source All Purpose Crystallography Software Package. *J. Appl. Crystallogr.* **2013**, *46*, 544−549.

(14) Momma, K.; Izumi, F. VESTA 3 for Three-dimensional Visualization of Crystal, Volumetric and Morphology Data. *J. Appl. Crystallogr.* **2011**, *44*, 1272−1276.

(15) Frisch, M. J.; Trucks, G. W.; Schlegel, H. B.; Scuseria, G. E.; Robb, M. A.; Cheeseman, J. R.; Scalmani, G.; Barone, V.; Petersson, G. A.; Nakatsuji, H.; Li, X.; Caricato, M.; Marenich, A. V.; Bloino, J.; Janes-ko, B. G.; Gomperts, R.; Mennucci, B.; Hratchian, H. P.; Ortiz, J. V.; Izmaylov, A. F.; Sonnenberg, J. L.; Williams-Young, D.; Ding, F.; Lipparini, F.; Egidi, F.; Goings, J.; Peng, B.; Petrone, A.; Henderson, T.; Ranasinghe, D.; Zakrzewski, V. G.; Gao, J.; Rega, N.; Zheng, G.; Liang, W.; Hada, M.; Ehara, M.; Toyota, K.; Fukuda, R.; Hasegawa, J.; Ishida, M.; Nakajima, T.; Honda, Y.; Kitao, O.; Nakai, H.; Vreven, T.; Throssell, K.; Montgomery, J. A., Jr.; Peralta, J. E.; Ogliaro, F.; Bearpark, M. J.; Heyd, J. J.; Brothers, E. N.; Kudin, K. N.; Staroverov, V. N.; Keith, T. A.; Kobayashi, R.; Normand, J.; Raghavachari, K.; Rendell, A. P.; Burant, J. C.; Iyengar, S. S.; Tomasi, J.; Cossi, M.; Millam, J. M.; Klene, M.; Adamo, C.; Cammi, R.; Ochterski, J. W.; Martin, R. L.; Morokuma, K.; Farkas, O.; Foresman, J. B.; Fox, D. J.*Gaussian 16*, revision A.03; Gaussian, Inc.: Wallingford CT, 2016.

(16) Adamo, C.; Barone, V. Toward Reliable Density Functional Methods without Adjustable Parameters: The PBE0Model. *J. Chem. Phys.* **1999**, *110*, 6158−6170.

(17) Grimme, S.; Ehrlich, S.; Goerigk, L. Effect of the Damping Function in Dispersion Corrected Density Functional Theory. *J. Comput. Chem.* **2011**, *32*, 1456−1465.

(18) Weigend, F.; Ahlrichs, R. Balanced Basis Sets of Split Valence, Triple Zeta Valence and Quadruple Zeta Valence Quality for H to Rn: Design and Assessment of Accuracy. *Phys. Chem. Chem. Phys.* **2005**, *7*, 3297−3305.

(19) Weigend, F. Accurate Coulomb-fitting Basis Sets for H to Rn. *Phys. Chem. Chem. Phys.* **2006**, *8*, 1057−1065.

(20) Turner, M. J.; McKinnon, J. J.; Wolff, S. K.; Grimwood, D. J.; Spackman, P. R.; Jayatilaka, D.; Spackman, M. A. *Crystal Explorer17*; University of Western Australia, 2017.

(21) Gándara, F.; Furukawa, H.; Lee, S.; Yaghi, O. M. High Methane Storage Capacity in Aluminum Metal-Organic Frameworks. *J. Am. Chem. Soc.* **2014**, *136*, 5271−5274.

(22) Currie, K.; Kropf, J.; Lee, T.; Blomgren, P.; Xu, J.; Zhao, Z.; Gallion, S.; Whitney, A.; Maclin, D.; Lansdon, E.; Maciejewski, P.; Rossi, A.; Rong, H.; Macaluso, J.; Barbosa, J.; Paolo, J.; Mitchell, S. Discovery of GS-9973, a Selective and Orally Efficacious Inhibitor of Spleen Tyrosine Kinase. *J. Med. Chem.* **2014**, *57*, 3856−3873.

(23) Parent, R. P.; Nakazono, T.; Lin, S.; Utsunomiya, S.; Sakai, K. Mechanism of Water Oxidation by Non-heme Iron Catalysts When Driven with Sodium Periodate. *Dalton Trans.* **2014**, *43*, 12501−12513.

(24) Grimvall, S. The Crystal Structure of $NaHSO_4H_2O$. *Acta Chem. Scand.* **1971**, *25*, 3213−3219.

(25) Pauling, L. *The Nature of the Chemical Bond*, 3rd ed.; Cornell University Press: Ithaca, NY, 1960; pp 320−321.

(26) Janesko, B. G.; Fisher, H. C.; Bridle, M. J.; Montchamp, J.-L. P(=O)H to P-OH Tautomerism: A Theoretical and Experimental Study. *J. Org. Chem.* **2015**, *80*, 10025−10032.

(27) Pietro, W. J.; Hehre, W. J. Tautomerization of Dimethyl Phosphonate. *J. Am. Chem. Soc.* **1982**, *104*, 3594−3595.

(28) Lee, S.; Bürgi, H.-B.; Alshmimri, S. A.; Yaghi, O. M. Impact of Disordered Guest-Framework Interactions on the Crystallography of Metal-Organic Frameworks. *J. Am. Chem. Soc.* **2018**, *140*, 8958−8964.

(29) Estimated from densities of common solvents. The estimated values are found to be consistent with our experimental observations (SI Table S3).

(30) Prince, E.; Finger, L.; Konnert, J. Constraints and Restraints in Refinement. *International Tables for Crystallography*, 3rd ed.; John Wiley & Sons, Inc.: New York, 2006; Vol. *A*, pp 694−701.

(31) Spackman, M. A.; Jayatilaka, D. Hirshfeld Surface Analysis. *CrystEngComm* **2009**, *11*, 19−32.

(32) McKinnon, J. J.; Spackman, M. A.; Mitchell, A. S. Novel Tools for Visualizing and Exploring Intermolecular Interactions in Molecular Crystals. *Acta Crystallogr., Sect. B: Struct. Sci.* **2004**, *60*, 627−668.

H